Draft version July 11, 2022
Typeset using LaTeX **twocolumn** style in AASTeX631

# Study of the dynamics of the Local Group using N-body Cosmological simulations

Author: Adrián Santander Garrote,[1]
Advisor: Jordi Miralda Escudé

[1] *Facultat de Física, Universitat de Barcelona*
*Diagonal 645, 08028 Barcelona, Spain*

## ABSTRACT

The Gaia satellite has been a revolution for the photometry and astrometry fields, providing a large amount of data (positions, parallaxes, proper motions) for the Local Group objects with a high accuracy never seen before. The goal of this work is to study the dynamics history of the Local Group galaxies from now to near to the time at the Big Bang using N-body simulations and taking advantage of the new proper motions measurements recently provided by Gaia. In order to obtain the 3D motion back in time of each Local Group galaxy, we have programmed an original N-body code in Fortran 90 which implements the Leapfrog algorithm which allows to solve numerically the equations of motion in classical mechanics for self-gravitating systems. We have done an exhaustive search in the literature to find the largest number of Local Group galaxies with updated measured proper motions and radial velocities. We have found a sample of 67 Local Group galaxies including the prominent members: the Milky Way, M31 and M33; and its dwarf satellites. We have transformed the right ascension, declination, heliocentric distance, line of sight velocity and proper motions obtained from the literature for all our sample of 67 galaxies into 6D phase-space coordinates in a Galactocentric reference system. We have run several N-body simulations with our code and our galaxy sample, and we have obtained the orbits back in time for 24 galaxies selected of the sample of 67 galaxies following two criteria: galaxies more distant than 50 kpc and with an error of their transverse velocity smaller than 50 km/s. Moreover, we have performed N-body simulations using only the Milky Way, M31 and M33 and we have compared the resulting orbits back in time. In addition, we have reviewed and described different important methods used to study some features of the dynamics of the Local Group, like the "Least Action Principle" or the "Timing Argument" which allows to estimate the mass of the Local Group.

*Keywords:* Local Group — Dwarf galaxy — N-body simulations— Leapfrog algorithm — Timing Argument — Least Action Principle

## 1. INTRODUCTION

The Local Group is a galaxy group with a diameter around 3 Mpc where our galaxy, the Milky Way (MW), is located. It is formed by other two large spiral galaxies, the Andromeda galaxy or M31 and M33, which dominate the dynamics of the Local Group with the Milky Way. Apart from these galaxies, about 100 dwarf galaxies are known which are satellite galaxies of the three dominant galaxies. The dwarf galaxies play an important role in the context of the $\Lambda$ Cold Dark Matter model ($\Lambda$ CDM) because it is thought that they are the first galaxies formed and the responsible in forming through mergers the large galaxies that it is observed nowadays so, the study of these objects can allow to reveal information about the primitive Universe. The dwarf galaxies can be classified into two different morphological classes: dwarf irregulars (dIrrs) and dwarf ellipticals (dEs). Another interesting characteristic to study is that these galaxies are highly dark matter dominated.

The study of the dynamics of the Local Group from now to the time at the Big Bang can reveal more information in favour of expansionary cosmological theories. Over the years, many studies of the kinematics and dynamics of the Local Group have been performed using different methods. One method used with important

results obtained is the "Timing Argument". The "Timing Argument" was first developed by Kahn & Woltjer (1959) and can be used to infer the total mass of the Local Group. The first assumption performed by Kahn & Woltjer (1959) was that approximately only the mass of the Milky Way and M31 contribute to the total mass of the Local Group, so they only took into account these two galaxies. Then they assumed that at the time of the Big Bang the Milky Way and M31 were very close each other and as the Universe expands after the Big Bang, the Milky Way and M31 has to travel away from each other in the Hubble Flow and only their expansion would reverse if they would have the enough mass in the present so knowing the age of the Universe and their present separation and velocity approach, it is possible to obtain the mass solving the equation of motion which is deduced below:

Under the assumption of the Friedmann-Lemaitre-Robertson-Walker (FLRW) model according to which the distribution of matter in the Universe is isotropic and homogeneous, the relative motion $r$ between two mass-less particles in a flat Universe can be described by the Friedmann equation:

$$\frac{\ddot{r}}{r} = \frac{-4\pi G\rho}{3} + \frac{\Lambda c^2}{3}, \tag{1}$$

where $c$ is the speed of light, $G$ is the universal gravitation constant, $\rho$ is the density of the Universe and $\Lambda$ is the cosmological constant. Then Kahn & Woltjer (1959) modified the equation (1) adding the gravity of the Local Group galaxies and rewrote the expression:

$$\ddot{r} = \frac{-GM}{r^2} + H_o^2 \Omega_\Lambda r, \tag{2}$$

where $H_o$ is the Hubble constant, $\Omega_\Lambda = \Lambda c^2/3(H_o)^2$ and $M$ is the mass of the Local Group that in this case it is assumed to be the sum of the Milky Way mass and the M31 mass.

The "Timing argument" has been used in many studies with different variations (e.g., Peñarrubia et al. (2014); Benisty et al. (2022)).

Another important field of study related with the study of the dynamics of the Local Group is the growing mode of the initial density field. Due that the present distribution of galaxies and their peculiar motions are the result of the gravitational amplification of the initial density fluctuation, it is possible to obtain the growing mode from the present distribution of galaxies. The method most used is the "Least Action Principle" which consists in obtaining the equations of motion from the stationary variations of the action of the system of particles with respect to orbits subject to fixed final positions. This can be done minimizing the action with respect to the coefficients of an expansion of the orbits in terms of functions that depend in time (Peebles 1989). Many studies have been used the "Least Action Principle" to obtain the orbits back in time of the Local Group galaxies (e.g., Peebles et al. (2011); Peebles & Tully (2013); Dunn & Laflamme (1993)).

This work is organized as follows: In section (2) the data used for this analysis is explained and it is presented the sample of galaxies. In section (3) the method used to build the N-body simulations is presented as well as its implementation. In section (4) are presented the results obtained as well as a discussion about them. Finally, the conclusions are in section (5).

## 2. DATA

In order to perform the N-body simulations, the algorithm needs to start with the initial conditions in the 6D phase-space (i.e., 3D initial positions and 3D initial velocities) of each galaxy (see section (3)).

To obtain the 6D phase-space it is necessary to know the current measurements of the distances, proper motions, radial velocities or line of sight velocities, and two celestial coordinates like the right ascension (RA) and declination (DEC) (Equatorial coordinate system).

The galaxy radial velocities can be measured with a high accuracy using high resolution spectrum, comparing the measured spectral lines with the spectral lines measured in the laboratory and applying the Doppler effect.

The galaxy distances are more difficult to determinate with a high accuracy. Recent studies have measured extragalactic distances using variable stars as an indicators like the Cepheids stars (Ripepi et al. 2022) or the RR Lyrae stars (Cusano et al. 2021). These stars have changes in their radius and in their absolute magnitudes. The principal characteristic of these stars is that their periods of the variability are related with their luminosities. With these period-luminosity relations it is possible to obtain their absolute magnitudes and with the measured apparent magnitudes it is possible to infer the distance using the distance modulus formula.

The proper motions are the most difficult to measure and usually these measurements have big uncertainties specially for the distant galaxies. This makes them the main source of error in the N-body simulations. However, in the recent years the Gaia mission has revolutionized the astrometry field greatly improving the precision and quantity of measurements of the objects near to the Milky Way. With the release of the proper motions Gaia catalogs (Gaia DR2, Gaia EDR3) it has been possible the measurement of systemic proper mo-

tions of nearly all the Milky Way dwarf satellite galaxies (Pace et al. (2022); McConnachie et al. (2021); Battaglia et al. (2021); McConnachie & Venn (2020)). There are also recent studies that measure proper motions from the Hubble Space Telescope (HST) data (Richstein et al. (2022); Van der Marel et al. (2012)).
In order to obtain the necessary measurements to compute the initial conditions in the 6D phase-space, an exhaustive search in the literature has been done to find the most possible amount of Local Group galaxies with the needed measurements and also it has searched the most updated information to improve the accuracy of the results.

**Table 1**. Main properties and adopted observational measurements for the sample of the Local Group galaxies analyzed in this work. Columns: (1) galaxy name, (2) right ascension, (3) declination, (4) heliocentric distance, (5) radial velocity, (6) proper motion in right ascension, (7) proper motion in declination, (8) references: (1) (Pace et al. 2022); (2) (Battaglia et al. 2021); (3) (Gaia Collaboration et al. 2021); (4) (Pawlowski & Tony Sohn 2021).

| Galaxy | RA | DEC | d | $v_{los}$ | $\mu_\alpha \cos\delta$ | $\mu_\delta$ | References |
|---|---|---|---|---|---|---|---|
| | (º) | (º) | (kpc) | (km $s^{-1}$) | (mas $yr^{-1}$) | (mas $yr^{-1}$) | |
| Antlia II | 143.8868 | -36.7673 | 132.0 ± 6.0 | 290.7 ± 0.5 | -0.093 ± 0.008 | 0.100 ± 0.009 | (1) |
| Aquarius II | 338.4813 | -9.3274 | 107.9 ± 3.3 | -71.1 ± 2.5 | -0.170 ± 0.119 | -0.466 ± 0.096 | (1) |
| Bootes I | 210.0200 | 14.5135 | 66.0 ± 3.0 | 101.8 ± 0.7 | -0.385 ± 0.017 | -1.068 ± 0.013 | (1) |
| Bootes II | 209.5141 | 12.8553 | 42.0 ± 2.0 | -117.0 ± 5.2 | -2.426 ± 0.080 | -0.414 ± 0.061 | (1) |
| Bootes III | 209.3000 | 26.8000 | 46.5 ± 2.0 | 197.5 ± 3.8 | -1.176 ± 0.019 | -0.890 ± 0.015 | (1) |
| Canes Venatici I | 202.0091 | 33.5521 | 210.0 ± 6.0 | 30.9 ± 0.6 | -0.096 ± 0.031 | -0.116 ± 0.020 | (1) |
| Canes Venatici II | 194.2927 | 34.3226 | 160.0 ± 4.5 | -128.9 ± 1.2 | -0.124 ± 0.117 | -0.254 ± 0.082 | (1) |
| Carina I | 100.4065 | -50.9593 | 105.6 ± 5.4 | 222.9 ± 0.1 | 0.532 ± 0.007 | 0.127 ± 0.006 | (1) |
| Carina II | 114.1066 | -57.9991 | 37.4 ± 0.4 | 477.2 ± 1.2 | 1.885 ± 0.019 | 0.133 ± 0.019 | (1) |
| Carina III | 114.6298 | -57.8997 | 27.8 ± 0.6 | 284.6 ± 3.25 | 3.095 ± 0.041 | 1.395 ± 0.045 | (1) |
| Columba I | 82.8570 | -28.0425 | 183.0 ± 10.0 | 153.7 ± 4.9 | 0.169 ± 0.073 | -0.400 ± 0.079 | (1) |
| Coma Berenices I | 186.7454 | 23.9069 | 42.0 ± 1.5 | 98.1 ± 0.9 | 0.423 ± 0.027 | -1.721 ± 0.024 | (1) |
| Crater I | 174.0660 | -10.8778 | 145.2 ± 4.0 | 149.3 ± 1.2 | -0.040 ± 0.120 | -0.120 ± 0.100 | (2) |
| Crater II | 177.3100 | -18.4130 | 117.5 ± 1.1 | 87.5 ± 0.4 | -0.072 ± 0.020 | -0.112 ± 0.013 | (1) |
| Draco I | 260.0684 | 57.9185 | 75.8 ± 5.4 | -290.7 ± 0.75 | 0.044 ± 0.006 | -0.188 ± 0.006 | (1) |
| Draco II | 238.1983 | 64.5653 | 21.5 ± 0.4 | -342.5 ± 1.15 | 1.027 ± 0.067 | 0.887 ± 0.072 | (1) |
| Eridanus II | 56.0925 | -43.5329 | 366.0 ± 17.0 | 75.6 ± 1.3 | 0.125 ± 0.101 | 0.013 ± 0.127 | (1) |
| Fornax I | 39.9583 | -34.4997 | 147.2 ± 8.4 | 55.2 ± 0.1 | 0.381 ± 0.001 | -0.359 ± 0.002 | (1) |
| Grus I | 344.1660 | -50.1680 | 127.0 ± 6.0 | -140.5 ± 2.0 | 0.069 ± 0.051 | -0.248 ± 0.072 | (1) |
| Grus II | 331.0250 | -46.4420 | 55.0 ± 2.0 | -110.0 ± 0.5 | 0.384 ± 0.033 | -1.484 ± 0.040 | (1) |
| Hercules I | 247.7722 | 12.7852 | 130.6 ± 6.1 | 45.0 ± 1.1 | -0.035 ± 0.042 | -0.339 ± 0.036 | (1) |
| Horologium I | 43.8813 | -54.1160 | 79.0 ± 4.0 | 112.8 ± 2.55 | 0.847 ± 0.035 | -0.607 ± 0.035 | (1) |
| Horologium II | 49.1077 | -50.0486 | 78.0 ± 8.0 | 168.7 ± 12.9 | 0.980 ± 0.190 | -0.840 ± 0.230 | (2) |
| Hydra II | 185.4251 | -31.9860 | 151.0 ± 8.0 | 303.1 ± 1.4 | -0.394 ± 0.140 | 0.00 ± 0.104 | (1) |
| Hydrus I | 37.3890 | -79.3089 | 27.6 ± 0.5 | 80.4 ± 0.6 | 3.781 ± 0.016 | -1.496 ± 0.015 | (1) |
| IC1613 | 16.1992 | 2.1178 | 758.0 ± 3.0 | -234.0 ± 0.6 | 0.040 ± 0.020 | 0.010 ± 0.010 | (2) |
| Leo I | 152.1146 | 12.3059 | 258.2 ± 9.5 | 282.9 ± 0.5 | -0.050 ± 0.014 | -0.120 ± 0.010 | (1) |
| Leo II | 168.3627 | 22.1529 | 233.0 ± 15.0 | 78.5 ± 0.6 | -0.109 ± 0.028 | -0.150 ± 0.026 | (1) |
| Leo IV | 173.2405 | -0.5453 | 151.4 ± 4.4 | 132.3 ± 1.4 | -0.009 ± 0.152 | -0.279 ± 0.115 | (1) |
| Leo V | 172.7857 | 2.2194 | 169.0 ± 4.4 | 173.0 ± 0.9 | 0.113 ± 0.219 | -0.391 ± 0.155 | (1) |
| Leo A | 149.8604 | 30.7464 | 717.0 ± 17.0 | 26.2 ± 1.0 | -0.060 ± 0.090 | -0.060 ± 0.090 | (2) |
| Leo T | 143.7292 | 17.0482 | 409.0 ± 28.0 | 38.1 ± 2.0 | 0.230 ± 0.370 | -0.120 ± 0.220 | (2) |
| LMC | 81.2800 | -69.7800 | 51.0 ± 2.0 | 262.2 ± 3.4 | 1.761 ± 0.447 | 0.304 ± 0.638 | (3) |
| M31 | 10.6850 | 41.2690 | 779.0 ± 18.5 | -300.1 ± 3.9 | 0.049 ± 0.011 | -0.037 ± 0.008 | (4) |
| M33 | 23.4621 | 30.6603 | 912.0 ± 12.0 | -180.0 ± 3.0 | 0.062 ± 0.004 | 0.011 ± 0.003 | (2) |
| NGC147 | 8.3010 | 48.5090 | 712.0 ± 20.0 | -193.1 ± 0.8 | 0.023 ± 0.014 | 0.038 ± 0.015 | (4) |
| NGC185 | 9.7420 | 48.3370 | 620.0 ± 18.5 | -203.8 ± 1.1 | 0.024 ± 0.014 | 0.006 ± 0.015 | (4) |
| NGC3109 | 150.7787 | -26.1597 | 1300.0 ± 47.0 | 403.0 ± 2.0 | -0.040 ± 0.030 | -0.010 ± 0.030 | (2) |

**Table 1** *continued*

**Table 1** *(continued)*

| Galaxy | RA | DEC | d | $v_{los}$ | $\mu_\alpha \cos\delta$ | $\mu_\delta$ | References |
|---|---|---|---|---|---|---|---|
| | (º) | (º) | (kpc) | (km $s^{-1}$) | (mas $yr^{-1}$) | (mas $yr^{-1}$) | |
| NGC6822 | 296.2358 | -14.7892 | 469.0 ± 36.0 | -54.5 ± 1.7 | -0.060 ± 0.010 | -0.070 ± 0.010 | (2) |
| Pegasus III | 336.1074 | 5.4150 | 215.0 ± 12.0 | -222.9 ± 2.6 | -0.030 ± 0.210 | -0.580 ± 0.213 | (1) |
| Peg-dIrr | 352.1512 | 14.7431 | 758.0 ± 69.0 | -179.5 ± 1.5 | 0.150 ± 0.140 | 0.070 ± 0.120 | (2) |
| Phoenix | 27.7762 | -44.4447 | 409.0 ± 22.0 | -21.2 ± 1.0 | 0.080 ± 0.030 | -0.060 ± 0.040 | (2) |
| Phoenix II | 354.9960 | -54.4115 | 84.1 ± 8.0 | 32.4 ± 3.75 | 0.507 ± 0.048 | -1.199 ± 0.058 | (1) |
| Pisces II | 344.6345 | 5.9526 | 183.0 ± 15.0 | -226.5 ± 2.7 | 0.681 ± 0.309 | -0.645 ± 0.215 | (1) |
| Reticulum II | 53.9203 | -54.0513 | 31.4 ± 1.4 | 64.3 ± 1.2 | 2.377 ± 0.024 | -1.379 ± 0.026 | (1) |
| Reticulum III | 56.3600 | -60.4500 | 92.0 ± 13.0 | 274.2 ± 7.45 | 0.260 ± 0.144 | -0.502 ± 0.226 | (1) |
| Sagittarius II | 298.1687 | -22.0681 | 70.2 ± 5.0 | -177.2 ± 0.55 | -0.769 ± 0.035 | -0.903 ± 0.023 | (1) |
| Sculptor I | 15.0183 | -33.7186 | 83.9 ± 1.5 | 111.4 ± 0.1 | 0.100 ± 0.002 | -0.158 ± 0.002 | (1) |
| Segue I | 151.7504 | 16.0756 | 23.0 ± 2.0 | 208.5 ± 0.9 | -2.102 ± 0.051 | -3.375 ± 0.046 | (1) |
| Segue II | 34.8226 | 20.1624 | 36.6 ± 2.45 | -40.2 ± 0.9 | 1.446 ± 0.059 | -0.322 ± 0.050 | (1) |
| Sextans I | 153.2628 | -1.6133 | 92.5 ± 2.5 | 224.3 ± 0.1 | -0.409 ± 0.009 | 0.037 ± 0.009 | (1) |
| Sextans A | 152.7533 | -4.6928 | 1425.0 ± 78.0 | 324.0 ± 1.0 | -0.150 ± 0.050 | -0.030 ± 0.050 | (2) |
| Sextans B | 150.0004 | 5.3322 | 1445.0 ± 79.0 | 304.0 ± 1.0 | -0.290 ± 0.160 | -0.280 ± 0.170 | (2) |
| Sg-dIrr | 292.4958 | -17.6808 | 1066.0 ± 88.0 | -78.4 ± 1.6 | 0.110 ± 0.190 | -0.370 ± 0.170 | (2) |
| SMC | 12.8000 | -73.1500 | 64.0 ± 4.0 | 145.6 ± 0.6 | 0.732 ± 0.373 | -1.226 ± 0.299 | (3) |
| Triangulum II | 33.3252 | 36.1702 | 28.4 ± 1.6 | -381.7 ± 1.1 | 0.575 ± 0.060 | 0.112 ± 0.069 | (1) |
| Tucana II | 342.9796 | -58.5689 | 58.0 ± 3.0 | -129.1 ± 3.5 | 0.911 ± 0.026 | -1.280 ± 0.029 | (1) |
| Tucana III | 359.1075 | -59.5833 | 22.9 ± 0.9 | -102.3 ± 0.4 | -0.048 ± 0.036 | -1.638 ± 0.039 | (1) |
| Tucana IV | 0.7170 | -60.8300 | 47.0 ± 4.0 | 15.9 ± 1.75 | 0.534 ± 0.053 | -1.707 ± 0.055 | (1) |
| Tucana V | 354.3470 | -63.2660 | 55.0 ± 5.5 | 36.2 ± 2.35 | -0.161 ± 0.176 | -1.157 ± 0.195 | (1) |
| UGC4879 | 139.0092 | 52.8400 | 1324.0 ± 79.0 | -29.2 ± 1.6 | -0.000 ± 0.110 | -0.040 ± 0.090 | (2) |
| Ursa Major I | 158.7706 | 51.9479 | 97.3 ± 5.85 | -55.3 ± 1.4 | -0.401 ± 0.036 | -0.613 ± 0.042 | (1) |
| Ursa Major II | 132.8726 | 63.1335 | 34.7 ± 2.1 | -116.5 ± 1.9 | 1.731 ± 0.021 | -1.906 ± 0.025 | (1) |
| Ursa Minor I | 227.2420 | 67.2221 | 76.2 ± 4.2 | -247.0 ± 0.4 | -0.120 ± 0.005 | 0.071 ± 0.005 | (1) |
| Willman 1 | 162.3436 | 51.0501 | 38.0 ± 7.0 | -12.8 ± 1.0 | 0.255 ± 0.087 | -1.110 ± 0.095 | (1) |
| WLM | 0.4925 | -15.4608 | 933.0 ± 34.0 | -130.0 ± 1.0 | 0.090 ± 0.030 | -0.070 ± 0.020 | (2) |

Pace et al. (2022) combine Gaia EDR3 astrometry with accurate photometry and utilize a probabilistic mixture model to measure the systemic proper motions of 52 Milky Way satellite galaxies.

The main used source is Pace et al. (2022) which contains the updated proper motions of almost all the Milky Way dwarf galaxies. Moreover, it has used the data of Battaglia et al. (2021), Gaia Collaboration et al. (2021) and Pawlowski & Tony Sohn (2021) to complete the Local Group galaxies sample with the data of the Large and Small Magellanic Cloud (LMC, SMC), M33, M31 and some M31 dwarf satellite galaxies; making a total of 67 Local Group galaxies. The adopted data of the galaxy sample are presented in Table (1).

With all the data of Table (1), it was calculated the 3D positions and the 3D velocities for all the galaxies of the sample using the coordinates library of the python package "astropy" (Robitaille et al. 2013). This library performs a series of matrix rotations and translations to convert positions and velocities in equatorial coordinates (RA, DEC, heliocentric distances, radial velocities, proper motions) into positions and velocities in Cartesian Galactocentric coordinates (x,y,z,vx,vy,vz). The reference system of the Galactocentric coordinates is centered in the Milky Way, x-axis points from the Sun's position to the center of the Milky Way, y-axis points towards the galactic longitude and z-axis points towards the galactic North Pole. The library takes by default the following values of the Sun´s position and velocity: $v_o = (11.10, 245.00, 7.25)\ km/s$, $R_o = 8.1\ kpc$, $z_o = 25\ pc$. After that, the Cartesian Galactocentric coordinates were transformed into coordinates respect to the center of mass of the galaxy system used in each simulation, using the equations (17) and (18).

Apart from the initial conditions in the 6D phase-space, to run the N-body simulations and to compute the past orbits of the galaxy system is necessary to know the mass of the involved galaxies (see section (3)).

The mass of the galaxies is another parameter difficult to measure specially for the dwarf satellite galaxies which are assumed to have an important amount of dark matter which we cannot measure directly. However, the

mass for the most important galaxies of the Local group (the Milky Way, M31, M33) can be inferred by modelling the kinematics of tracers (halo stars, globular clusters, satellite galaxies) around it.

The values of the masses of the galaxy sample are taken from the most recent measurements: $1.17^{+0.21}_{-0.15} \times 10^{12} M_o$ for the Milky Way (Callingham et al. 2019), $1.8 \pm 0.5 \times 10^{12} M_o$ for M31 (Shull 2014), $5.0 \pm 1.0 \times 10^{11} M_o$ for M33 (Corbelli et al. 2014), $1.8 \pm 0.4 \times 10^{11} M_o$ for the LMC (Benisty et al. 2022). As almost there are not mass measurements for the Local Group dwarf galaxies, a mass of $10^9 M_o$ was estimated for each dwarf galaxy of the sample. This is consistent with the known total mass of the Local Group: $3.7 \pm 0.5 \times 10^{12} M_o$ (Benisty et al. 2022).

## 3. METHOD

The N-body simulations presented in this work were conducted with an original implementation in Fortran 90 (Adams et al. 1992) of the Leapfrog algorithm which allows to solve numerically the equations of motion in classical mechanics to determine the dynamics of a system of N particles with a gravitational interaction.
In order to perform the simulations, the Local Group galaxies selected were treated as point mass particles which it is a good approximation for the most distances galaxies. Moreover, only was taking into account the gravitational interaction due that it is the unique fundamental interaction that acts significantly in large distances.

### 3.1. *Leapfrog integrator*

Leapfrog is a second order symplectic integrator which allows to solve numerically ordinary differential equations. Like others numerical integration methods, Leapfrog integration discretizes the integration domain of the differential equation in several intervals (steps) with the same width (integration step) and it solves numerically the differential equation for each step. Although this method is very simple it has used in many N-body simulations (e.g., Taheri et al. (2022)) due the advantages it has over other methods. Leapfrog only needs one copy of the physical state of the system and one force evaluation for step which allows to reduce the cost and computational time, and this is very important for N-body simulations where the cost of a force evaluation is very high. In addition, it is a symplectic integrator which means that it conserves specific properties to Hamiltonian systems like the total energy in systems with a time-independent Hamiltonian or the angular momentum in axisymmetric systems (see Fig. (1) and Fig. (2)). Leapfrog gives an exact solution to a discrete Hamiltonian system which it is a very good approximation of the continuum Hamiltonian (the real system), so it conserves exactly the energy of the discrete Hamiltonian and this energy oscillates around the value of the real energy of the system without numerical dissipation. This property it is very important to N-body simulations with self-gravitating systems because this allows to maintain stable the orbits that also are stable in the reality.
Leapfrog algorithm applied to the Newton's equations of motion results in the following equations (see Quinn et al. (1997)):

$$v_{i+1/2} = v_i + \frac{1}{2} a_i \triangle t, \tag{3}$$

$$r_{i+1} = r_i + v_{i+1/2} \triangle t, \tag{4}$$

$$v_{i+1} = v_{i+1/2} + \frac{1}{2} a_{i+1} \triangle t, \tag{5}$$

where $v_i$ is the velocity vector of a particle at the step i, $x_i$ is the position vector, $a_i$ is the acceleration vector, and $\triangle t$ is the time step, i.e., the time that elapses in each step. When several of these steps are put together, the algorithm allows to compute positions and velocities in interleaved steps and this leap over each other which gives the name of the algorithm, "Leapfrog". Substituting the equation (3) into (4) and into (5), it is obtained the following expressions:

$$r_{i+1} = r_i + v_i \triangle t + \frac{1}{2} a_i (\triangle t)^2, \tag{6}$$

$$v_{i+1} = v_i + \frac{1}{2} (a_i + a_{i+1}) \triangle t. \tag{7}$$

These last equations allow to compute positions and also velocities in integer steps. Another important property is that equations (6) and (7) are time reversible and this makes possible to calculate the positions and velocities of the particles in the past. This is obtained only changing the sign of $\triangle t$ ($\triangle t \rightarrow -\triangle t$) :

$$r_i = r_{i+1} - v_{i+1} \triangle t + \frac{1}{2} a_{i+1} (\triangle t)^2, \tag{8}$$

$$v_i = v_{i+1} - \frac{1}{2} (a_{i+1} + a_i) \triangle t. \tag{9}$$

In this way, putting present initial conditions for the positions in $r_{i+1}$ and for the velocities in $v_{i+1}$ it is obtained the positions and the velocities in one step in the past $r_i$ and $v_i$, respectively. Notice that the Eqs. (8) and (9) can be demonstrated substituting the expressions for $r_{i+1}$ and $v_{i+1}$ (Eqs. (6) and (7)).
Leapfrog integrator has an accuracy of second order which means that the overall error is proportional to $(\triangle t)^2$ when it is integrated over a finite time. This can

be easily demonstrated using a Taylor expansion of one time step $\triangle t$ around $t$ for the vector position $r(t)$:

$$r_{i+1}(t) = \sum_{n=0}^{\infty} \frac{(\triangle t)^n}{n!} \frac{dr^n(0)}{dt} = \tag{10}$$

$$= r_i + v_i \triangle t + \frac{1}{2} a_i (\triangle t)^2 + O(\triangle t^3). \tag{11}$$

Notice that the Taylor expansion of the vector position (Eq. (11)) coincides with the Leapfrog equation (Eq. (6)) at second order of the expansion.
Higher order numerical integration methods can be constructed from combinations of Leapfrog steps (Yoshida 1990). In addition, the Leapfrog integrator can be modified to vary the time steps for each particle in the N-body simulations (Quinn et al. 1997). For the purposes of this work the classic Leapfrog integrator is enough because the use of a higher order integrator does not improve significantly the accuracy of the N-body simulations.

### 3.2. *Basic equations of classical mechanics*

Due that only was taking into account the gravitational interaction in the N-body simulations, the equations needed to compute the orbits of the galaxies are the equations of motion of Newton.
The Newton's second law and the universal gravitational law are (Kibble & Berkshire 2004):

$$\vec{F_i} = m_i \vec{a_i}, \tag{12}$$

$$\vec{F_i} = \sum_{j=1, i \neq j}^{N} -G \frac{m_i m_j}{|\vec{r_i} - \vec{r_j}|^3} (\vec{r_i} - \vec{r_j}), \tag{13}$$

where $\vec{F_i}$ is the gravitational force that the particle $i$ experiences due to the gravitational interactions with the particles $j$, $N$ is the number of particles, $m$ is the mass of the particles, $\vec{r}$ is the position vector, $G$ is the universal gravitational constant ($6.67384 \cdot 10^{-11} Nm^2 kg^{-2}$ in the SI units), and $\vec{a_i}$ is the gravitational acceleration that the particle $i$ experiences,

$$\vec{a_i} = \sum_{j=1, i \neq j}^{N} -G \frac{m_j}{|\vec{r_i} - \vec{r_j}|^3} (\vec{r_i} - \vec{r_j}). \tag{14}$$

Others classical equations used in the simulations are the total angular momentum $\vec{L}$ and the mechanical energy $E$ of a self-gravitating system of classical particles:

$$\vec{L} = \sum_{i=1}^{N} m_i (\vec{r_i} \times \vec{v_i}), \tag{15}$$

$$E = T + U = \sum_{i=1}^{N} \frac{1}{2} m_i v_i^2 - \frac{1}{2} \sum_{i=1}^{N} \sum_{j=1, i \neq j}^{N} G \frac{m_i m_j}{|\vec{r_i} - \vec{r_j}|}, \tag{16}$$

where $v_i$ is the modulus of the velocity vector of each particle, $T$ is the kinetic energy and $U$ is the gravitational potential energy of the system of particles.
Finally, in order to work in the reference system respect to the center of mass of the sample of galaxies analyzed, the following equations were used:

$$\vec{r_{CM}} = \frac{1}{M} \sum_{i=1}^{N} m_i \vec{r_i}, \tag{17}$$

$$\vec{v_{CM}} = \frac{1}{M} \sum_{i=1}^{N} m_i \vec{v_i}, \tag{18}$$

where $M$ is the total mass of a system of $N$ particles while $m_i$ are the masses of each particle and $\vec{r_{CM}}$ and $\vec{v_{CM}}$ are the position vector and the velocity vector of the center of mass of the system, respectively.

### 3.3. *Algorithm implementation*

An original N-body code has been written in the computer language Fortran 90 to implement the Leapfrog integrator applied to the equations of motion in classical mechanics. The code is structured in several subroutines in order to improve the organization of the program in addition to a main program in which the initial conditions for each of the N particles in the N-body simulation (mass, positions, velocities) are inputted in vector form and in which the subroutines are called to run the simulation. In the main program, the initial positions and velocities are transformed into coordinates respect to the center of mass of the system of N particles using the equation (17) for the positions and the equation (18) for the velocities. The results obtained in the N-body simulations were saved in a 'data' file and the graphs of the results were performed by the free software, Gnuplot (Williams & Kelley 2010). In the following lines, the implementation of the subroutines is explained in detail.
The first subroutine receives as input a vector which contains the mass of each galaxy of the sample and a two-dimensional array which contains the positions so that each row corresponds to the position vector of one galaxy of the sample divided by three components separated in three columns. The velocity and acceleration vectors are implemented in the same way. Then, the subroutine applies the equation (14) and computes each component of the gravitational acceleration vector for all the galaxies, and it saves the results as output into two-dimensional array.
The second subroutine applies the equation (8) to compute the three components of the position vector for each galaxy after a time step into the past $r_i$. The input information are the components of the velocity vector $v_{i+1}$ and the position vector $r_{i+1}$ from the previous step for

each galaxy, the acceleration vector $a_{i+1}$ computed by the previous subroutine and the time step as integer. The output is an array with the updated positions.
The third subroutine computes the components of the vector velocity in the next step $v_i$ using the equation (9). Only needs as input the velocity $v_{i+1}$ and the acceleration vectors $a_{i+1}$ from the previous step, the time step and the acceleration vector of the current step $a_i$ which it can be re-calculated with the updated positions $r_i$ using again the first subroutine.
The last two subroutines compute the total angular momentum and the total energy of the galaxy system for one time step using the equations (15) and (16), respectively. The input parameters are the mass of each galaxy, the velocity and the position arrays in one determinate step.
All these subroutines are called in the main program inside a time loop in order to obtain the position of each galaxy in each time step during a determinate time towards the past which allows to determinate the orbits of the galaxies of the simulation from now to the past.

### 3.4. *N-body simulations performed*

Several different N-body simulations were performed in this work using the code explained in detail in subsection 3.3.
First of all, a simulation with only two particles was realized to test the code with 10000 steps, G = 1, $m_1 = m_2 = 1$ the mass of the particles, $\vec{r_1} = (-1, 0, 0)$ $\vec{r_2} = (1, 0, 0)$ the initial position vectors, $\vec{v_1} = (0, 0.5, 0)$ $\vec{v_2} = (0, -0.5, 0)$ the initial velocity vectors and $\triangle t = 0.01$ the time step, all these parameters in arbitrary units. These parameters were chosen to reproduce a circular orbit and test that the implemented Leapfrog algorithm conserves the mechanical energy and the total angular momentum of the system of two particles. The results of the test of the code are presented in subsection 3.5.
The following simulations were done with the sample of the Local Group galaxies. All these N-body simulations were performed during a total time interval of $12 \cdot 10^9$ years with a time step of $10^6$ years which it is close to the age of the Universe and it allows to compute the orbits back in time near to the time at the Big Bang. Moreover, it was used the universal gravitational constant expressed in these units: $G = 4.49234 \cdot 10^{-9} \frac{pc^3}{M_o \cdot kyear^2}$, so that it was used the initial position vectors expressed in parsecs (pc), the masses in solar masses ($M_o$) and the initial velocity vectors in pc/kyear. At first, it was realized only simulations with the three most massive galaxies of the Local Group which dominate the dynamics of the Local Group: the Milky Way, M31 and M33. It was realized one simulation with these galaxies with the initial velocity vectors calculated from the central value of the measured systemic proper motion of each galaxy and several simulations changing the initial velocity vectors by changing randomly the proper motions in the range of the measurement uncertainty in order to show how can change the orbits with the errors of the proper motions measurements which are the principal error source. Finally, one simulation was performed with the total sample of 67 Local Group galaxies. However, only the orbits of 24 galaxies are presented. These galaxies are the Milky Way, M31, M33, the LMC and the dwarf galaxies in the sample which are further than 50 kpc respect to the Sun and which have an uncertainty in the transverse velocity smaller than 50 km/s. The uncertainty in the transverse velocity $\delta v_T$ was estimated using the following equation:

$$\delta v_T = \delta\mu \cdot d, \tag{19}$$

where $\delta\mu$ is the uncertainty of the total proper motion and $d$ is the heliocentric distance of each dwarf galaxy. Notice that only was taking into account the errors of the proper motions due that are the principal error source. The results obtained are presented in section (4).

### 3.5. *Results of the test of the code*

The results obtained with the simulation with two particles to test the code are presented:

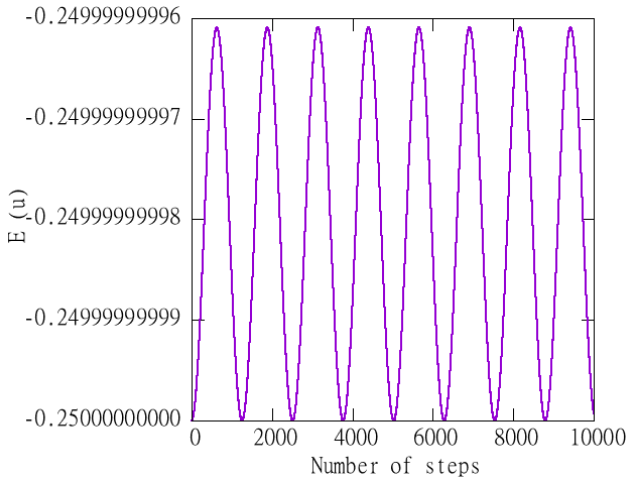


**Figure 1**: Mechanical energy E of the system in arbitrary units against the number of steps of the simulation.

In Fig. (1) and Fig. (2), it is observed that the mechanical energy and the angular momentum of the system of two particles with a circular orbit, both are conserved with the time and only they present a very small oscillations around the central value as expected in a simulation that implements the Leapfrog algorithm.

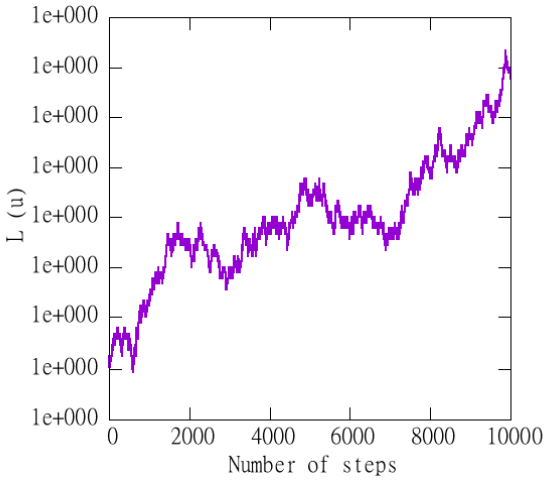


**Figure 2**: Angular momentum modulus of the system L in arbitrary units against the number of steps of the simulation.

## 4. RESULTS AND DISCUSSION

In this section are presented the main results obtained with the N-body simulations using our sample of Local Group galaxies as well as a discussion about them. In all the graphics the orange round dots represent the initial position of the galaxy in the simulation, i.e., the measured present position, while the blue square dots represent the last position in the past (near to the time at the Big Bang). Also, they are plotted black dots every $3 \cdot 10^9$ years or 3000 steps.

In Fig. (3) there are the results obtained with the N-body simulation using only the Milky Way, M31 and M33, it is observed a clear attraction between the Milky Way, M31 and M33 from close to the Big Bang to now. Comparing with the simulation performed with all the galaxies of the sample Fig. (5), it is observed changes in the orbits due probably for the interaction with the LMC since it is the fourth most massive galaxy of the Local Group. The main difference in the orbits in the plane x-y that we can appreciate comparing the two Figs. ((3), (5)) is that the MW and M31 start their movement travelling away from each other (Fig. (5)), although after this they recover the attraction trend observed in Fig. (3).

In addition, it is seen that M33 is located very far from the Milky Way and M31 at the time of the Big Bang and as time passes M33 approaches to the system MW-M31 with a positive acceleration (the black points are equidistant in the time but in M33 the points are farther from each other as the time passes) and it ends very close to M31 (the present position). This also happens in Fig. (5). In Fig. (4) are presented the results with the simulations performed using only the Milky Way, M31 and M33, changing the values of the initial velocities using different values for the proper motions which are inside the measurement error. The measurement errors of the proper motions of M31 and M33 are relatively small compared to the dwarf galaxies of the sample (see Table (1)). In Fig. (4) we can see how important is the accuracy of the proper motions measurements to obtain the correct orbits. We can observe that small variations in the proper motions can produce significantly changes in the orbits and these changes/errors in the orbits are amplified with the time. Moreover, it seems that the dispersion of the orbits is bigger in the plane x-z than in the plane x-y where we have used the same values of proper motions.

Finally, in Figs. (6), (7) and (8) are presented the results of the N-body simulations performed with the full sample of 67 Local Group galaxies. However, in the graphics only are represented the orbits of the 24 selected galaxies of the sample using the criteria explained in subsection 3.4. We can observe several orbits of dwarf galaxies that start very far from the principal galaxies of the Local Group (the MW, M31, M33) like the dwarf galaxies Ursa Minor I, Leo II, Leo I in Fig. (6) or Sagittarius II in Fig. (7) and in all cases they finish orbiting around the principal galaxies specially around the Milky Way since the most dwarf galaxies of the sample are MW satellites.

In addition, we can distinguish another type of dwarf galaxies that start their motion at the time close to the Big Bang very close to the MW and perform many orbits around it, this is the case of Ursa Major I (Fig. (8)), Sextans I (Fig. (7)) or the LMC (Fig. (8)), one of the dwarf galaxies nearer of the Milky Way. Moreover, we can observe how the LMC orbits around the MW as it moves.

Between these two types of dwarf galaxies, the dwarf galaxies that are further from MW-M31-M33 at the time close to the Big Bang have the most realistic orbits because the dwarf galaxies that remain close to MW-M31-M33 during all the simulation and have a lot of turns around the system, it is possible that these galaxies have suffered too many interactions with MW-M31-M33 which caused changes in their orbits.

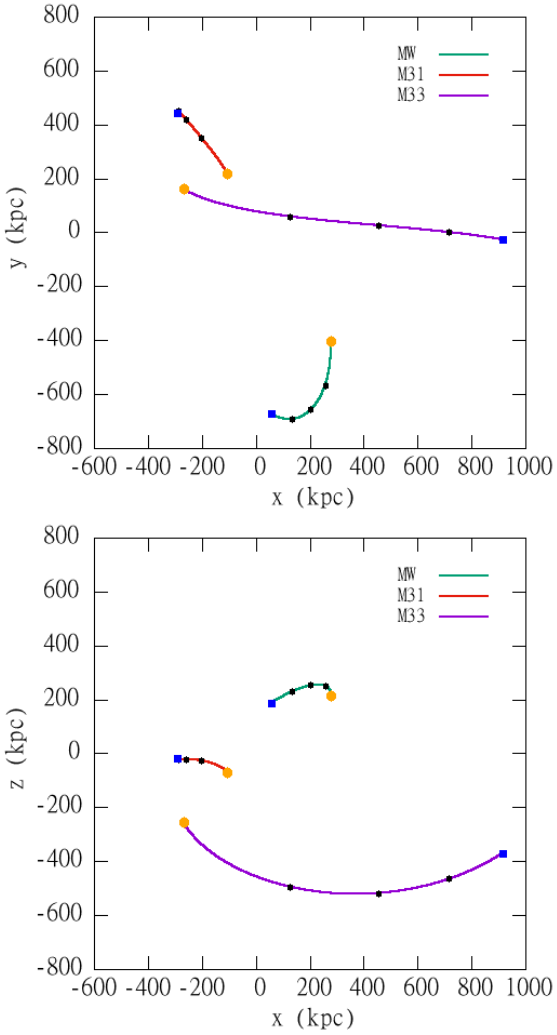


**Figure 3**: Orbits of the Milky Way, M31 and M33 in the plane x-y and in the plane x-z using Cartesian Galactocentric coordinates corrected respect to the position of the center of mass of the system. Results obtained from the simulation realized with only the Milky Way, M31 and M33.

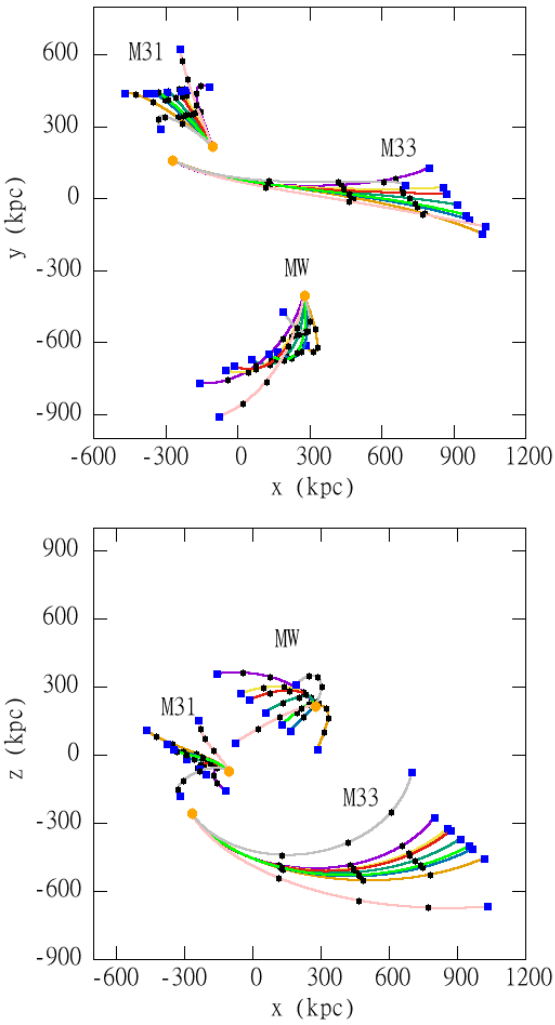


**Figure 4**: Orbits of the Milky Way, M31 and M33 in the plane x-y and in the plane x-z for different values of the proper motions using Cartesian Galactocentric coordinates corrected respect to the position of the center of mass of the system.

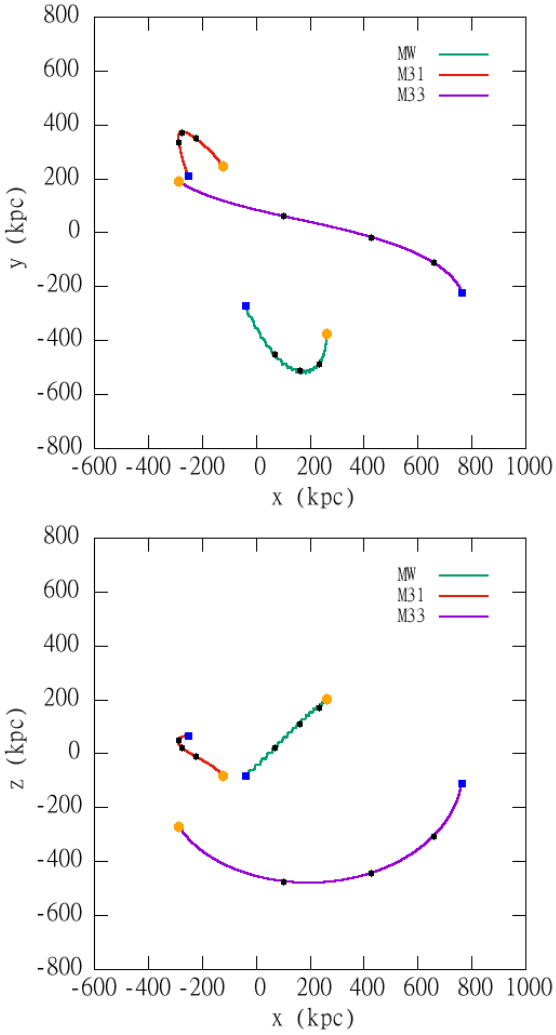


**Figure 5**: Orbits of the Milky Way, M31 and M33 in the plane x-y and in the plane x-z using Cartesian Galactocentric coordinates corrected respect to the position of the center of mass of the system. Results obtained from the simulation realized with 67 galaxies.

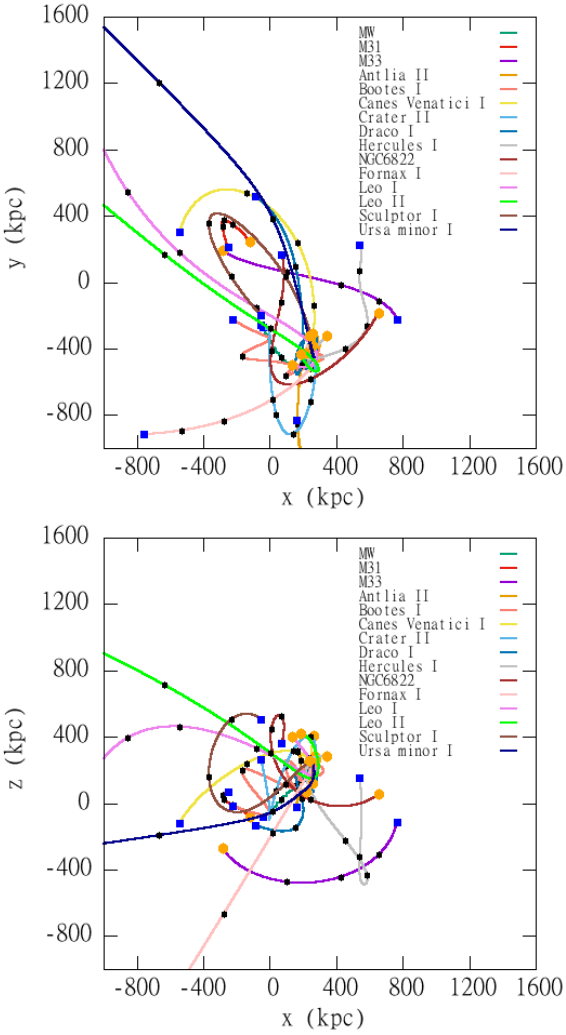


**Figure 6**: Orbits of some of the subsample of 24 galaxies in the plane x-y and in the plane x-z using Cartesian Galactocentric coordinates corrected respect to the position of the center of mass of the system. Results obtained from the simulation realized with 67 galaxies.

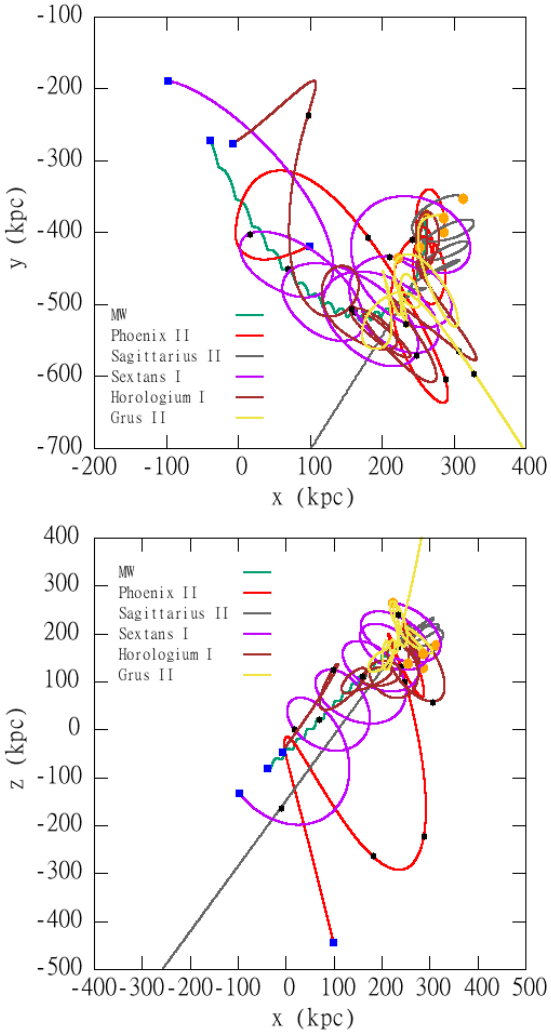


**Figure 7**: Orbits of some of the subsample of 24 galaxies in the plane x-y and in the plane x-z using Cartesian Galactocentric coordinates corrected respect to the position of the center of mass of the system. Results obtained from the simulation realized with 67 galaxies.

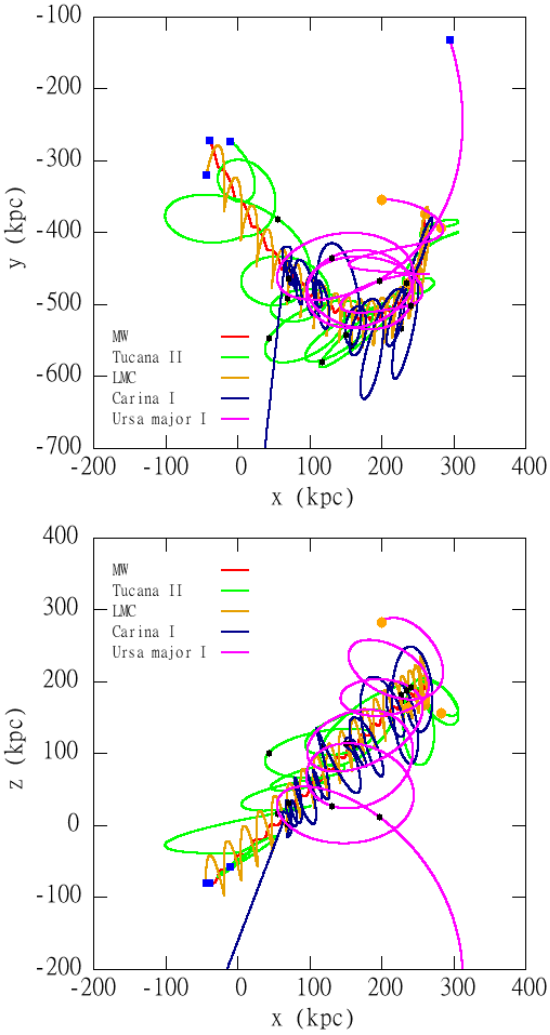


**Figure 8**: Orbits of some of the subsample of 24 galaxies in the plane x-y and in the plane x-z using Cartesian Galactocentric coordinates corrected respect to the position of the center of mass of the system. Results obtained from the simulation realized with 67 galaxies.

## 5. CONCLUSIONS

We have implemented a simple model to perform N-body simulations and to study the dynamics of the Local Group. This model has consisted in modeling the galaxies as point mass particles and using the simplest variety of the Leapfrog algorithm with a constant time step to solve the equations of motion from the estimated masses and the present positions and velocities measurements. With these considerations we have obtained the orbits back in time of our galaxies. Some interesting results found are the following: at the time of the Big Bang M33 is very far from the Milky Way and M31 instead of being close as we would think; the orbits of some dwarf galaxies like the LMC which performs many orbits around the Milky Way are less realistic than the orbits of the dwarf galaxies which start further because they have suffered less interactions; small changes in the proper motions can vary the orbit significantly. There are other variations of the Leapfrog algorithm like the variation of the time step during the simulation which can be interesting to compare with the algorithm that we have used. Also, it is possible to refine the model presented in this work by adding, for example, a spherical gravitational potential for the galaxies that are closer enough to notice their 3D structure. Another interesting refine of the model it is to add the external perturbations outside the Local Group than can create tidal disruptions in the system to compare the results obtained with our results. We leave all these open questions for future research works.

## ACKNOWLEDGMENTS

I would like to thank my advisor, Dr. Jordi Miralda for his support and his guidance during the realization of this work.

## REFERENCES

Adams, J. C., Brainerd, W. S., Martin, J. T., Smith, B. T., & Wagener, J. L. 1992, fortran 90 Handbook, Vol. 32 (McGraw-Hill New York)

Battaglia, G., Taibi, S., Thomas, G. F., et al. 2021, Astronomy & Astrophysics

Benisty, D., Vasiliev, E., Evans, N. W., et al. 2022, The Astrophysical Journal Letters, 928, L5

Callingham, T. M., Cautun, M., Deason, A. J., et al. 2019, Monthly Notices of the Royal Astronomical Society, 484, 5453

Corbelli, E., Thilker, D., Zibetti, S., Giovanardi, C., & Salucci, P. 2014, Astronomy & Astrophysics, 572, A23

Cusano, F., Moretti, M. I., Clementini, G., et al. 2021, MNRAS, 504, 1, doi: 10.1093/mnras/stab901

Dunn, A., & Laflamme, R. 1993, Monthly Notices of the Royal Astronomical Society, 264, 865

Gaia Collaboration, Luri, X., Chemin, L., et al. 2021, A&A, 649, A7, doi: 10.1051/0004-6361/202039588

Kahn, F. D., & Woltjer, L. 1959, ApJ, 130, 705, doi: 10.1086/146762

Kibble, T., & Berkshire, F. H. 2004, Classical mechanics (world scientific publishing company)

McConnachie, A. W., Higgs, C. R., Thomas, G. F., et al. 2021, Monthly Notices of the Royal Astronomical Society, 501, 2363

McConnachie, A. W., & Venn, K. A. 2020, Research Notes of the AAS, 4, 229

Pace, A. B., Erkal, D., & Li, T. S. 2022, arXiv e-prints, arXiv:2205.05699. https://arxiv.org/abs/2205.05699

Pawlowski, M. S., & Tony Sohn, S. 2021, ApJ, 923, 42, doi: 10.3847/1538-4357/ac2aa9

Peñarrubia, J., Ma, Y.-Z., Walker, M. G., & McConnachie, A. 2014, MNRAS, 443, 2204, doi: 10.1093/mnras/stu879

Peebles, P. 1989, The Astrophysical Journal, 344, L53

Peebles, P., & Tully, R. B. 2013, arXiv preprint arXiv:1302.6982

Peebles, P. J. E., Tully, R. B., & Shaya, E. J. 2011, arXiv e-prints, arXiv:1105.5596. https://arxiv.org/abs/1105.5596

Quinn, T., Katz, N., Stadel, J., & Lake, G. 1997, arXiv e-prints, astro. https://arxiv.org/abs/astro-ph/9710043

Richstein, H., Patel, E., Kallivayalil, N., et al. 2022, arXiv preprint arXiv:2204.01917

Ripepi, V., Chemin, L., Molinaro, R., et al. 2022, Monthly Notices of the Royal Astronomical Society, 512, 563

Robitaille, T. P., Tollerud, E. J., Greenfield, P., et al. 2013, Astronomy & Astrophysics, 558, A33

Shull, J. M. 2014, The Astrophysical Journal, 784, 142

Taheri, S., King, J. R., & Shumlak, U. 2022, Computer Physics Communications, 274, 108288, doi: 10.1016/j.cpc.2022.108288

Van der Marel, R. P., Fardal, M., Besla, G., et al. 2012, The Astrophysical Journal, 753, 8

Williams, T., & Kelley, C. 2010, Gnuplot, http://www.gnuplot. info, March

Yoshida, H. 1990, Physics letters A, 150, 262